

All-fiber microendoscopic polarization sensing at single-photon level aided by deep-learning

MARTIN BIELAK^{1, +}, DOMINIK VAŠINKA^{1, +}, AND MIROSLAV JEŽEK^{1, *}

¹Department of Optics, Faculty of Science, Palacký University, 17. listopadu 1192/12, 77900 Olomouc, Czechia

⁺ These authors contributed equally to this work

^{*} jezek@optics.upol.cz

Compiled May 6, 2024

The polarization of light conveys crucial information about the spatial ordering and optical properties of a specimen. However, precise polarization measurement in challenging conditions, including constrained spaces, low light levels, and high-speed scenarios, remains a severe challenge. Addressing this problem, we introduce a real-time polarization measurement method accurate down to a single-photon level that provides complete information about the polarization state. Free of moving components, the polarization sensor utilizes a few-mode fiber followed by a fiber array and a detector array. The calibration of the sensor relies on a neural network yielding unprecedented accuracy across all polarization states, including partially polarized light. We validate the approach by visualizing the polarization structure of a biological specimen. Our method offers an efficient and reliable solution for real-time polarization sensing and microendoscopy under low-light conditions.

1. INTRODUCTION

From ellipsometry to optical communications, from microscopy to sensing, light polarization represents a fundamental element across various scientific disciplines. In particular, the polarization of light emitted by an optically anisotropic specimen carries essential information about its material structure and optical properties. Consequently, conducting a thorough analysis of such specimens demands precise characterization of the emitted light polarization. While relatively straightforward in a controlled environment, accurate polarization measurement under challenging conditions remains a significant obstacle.

Low light intensities come with a reduced signal-to-noise ratio, complicating the extraction of meaningful polarization information from data burdened with environmental and shot noise. Similarly, conducting high-speed measurements is accompanied by a low number of detections within the acquisition time. While increasing the incident light intensity can help, it is limited by the photodamage threshold of the sample. Incorporating single-photon detectors can substantially improve the accuracy of indirect protocols relying on the number of detected photons for polarization state reconstruction. However, another

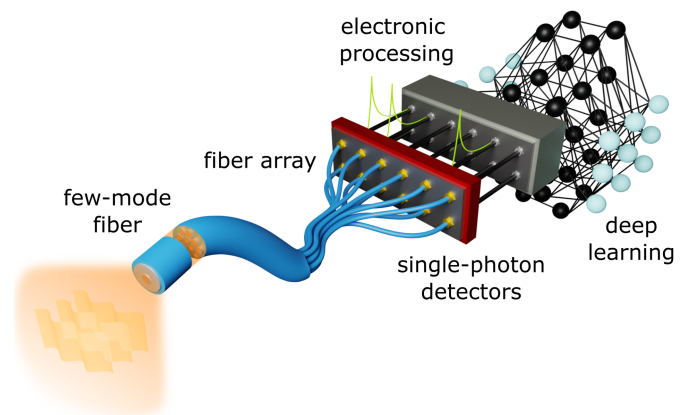


Fig. 1. A visual representation of the all-fiber polarization sensor. Polarized light emitted from a specimen is collected by a short piece of a few-mode fiber. The intermodal interference generates a granular speckle pattern at the output. Several isolated samples of this pattern impinge a fiber array and propagate to a corresponding number of single-photon detectors. The recorded detections are electronically processed using deep learning methods to characterize the incident polarization state.

drawback arises as these detectors are relatively large and cannot be efficiently integrated. This issue becomes particularly problematic when faced with the third condition - constrained space. Such spaces not only impose restrictions on the overall size of the measurement setup but also limit the placement and alignment of optical components. Therefore, challenging conditions pose a severe setback, especially for measurements during invasive medical procedures, such as microendoscopy. We address these problems by developing a polarization sensor based on light propagation in disordered media.

Coherent light propagating within a disordered medium is subjected to multimode interference, generating a granular speckle pattern. Despite the apparent degrading effect, the pattern retains encoded information about the incident light [1–4]. Analyzing the light propagation in disordered media and employing suitable post-processing techniques, one can study the disordering effects of the media [5, 6], estimate and classify input images [7–12], learn to modulate the input for project-

ing a targeted image on the output [13], reconstruct shapes of propagated ultrashort laser pulses [14, 15], compute and communicate [16–20], and even make an accurate spectrometer or wavemeter [21, 22]. Recently, the speckle pattern has proved to preserve a great deal of information about the polarization state of the incident light [23, 24]. Although additional studies successfully advancing the application of disordered-media propagation have been conducted [25–28], developing a compact polarimeter capable of ultra-fast measurements with single-photon sensitivity continues to be an open problem.

Here, we introduce a highly accurate single-shot all-fiber polarization sensor based on intermodal interference in a short piece of a few-mode fiber. Instead of processing the complete spatial speckle pattern, our approach relies on its sparse sampling in a few isolated points using a fiber array. Fiber-coupled single-photon detectors then allow for high sensitivity down to a single-photon level. The all-fiber sensor contains no moving components or complex metastructures and is sufficiently small for endoscopic procedures. Furthermore, the method can accurately operate at a high repetition rate, processing up to thousands of polarization states per second. The setup is aided by a deep machine-learning model reconstructing complete polarization information in real-time. The calibrated sensor maintains unparalleled accuracy and stability throughout an extensive period, even for partially-polarized light. We demonstrate the sensing abilities of our approach in polarized light imaging of dense connective tissue. Our polarization sensor opens new frontiers in precise polarization measurements, providing an indispensable tool for cutting-edge applications in biomedicine, material research, and beyond.

2. EXPERIMENTAL AND DATA PROCESSING SETUP

The speckle-based polarization sensor depicted in Fig. 1 employs a common few-mode fiber to characterize the input polarization state. The sensor collects light with a front face of a 5 cm long step-index SMF28 fiber with a numerical aperture of 0.14 and a core diameter of 8.2 μm . While the motivation behind choosing this specific fiber type is to minimize the sensing area, we emphasize that this preference is optional. Virtually any few-mode or multimode fiber, including significantly shorter variants, can be used as a substitute. The main requirement for the fiber is to support several interfering modes necessary for creating a polarization-dependent speckle pattern at the output. We collect discrete samples of this interference pattern using a fiber array comprising seven gradient multimode fibers, each with a 62.5 μm core diameter, forming a 375 μm diameter honeycomb pattern. Each fiber then propagates the collected intensity signal to an independent single-photon avalanche diode, recording the number of detection events. After normalizing the measured counts, this setup associates the sampled polarization state with the corresponding relative frequencies of each detector, which we term a count distribution.

Using the sensor, we analyzed 30,000 polarization states, uniformly covering the entire surface of the Poincaré sphere [29]. Our state preparation involved a laser beam with a central wavelength of 0.8 μm attenuated to the single-photon level and propagated through a linear polarizer. Subsequently, a twisted nematic liquid crystal device [30], controlled by voltage signals, performed a targeted unitary transformation of the polarization state. The device operation underwent calibration through bidirectional modeling [31], ensuring fast and precise preparation of arbitrary polarization states. Moreover, we expand our

dataset to include partially polarized light. We can establish a count distribution for a mixture of two orthogonal states by weight-summing their respective distributions. This approach is virtually equivalent to directly measuring the corresponding mixed state. Employing this method, we assembled an extensive dataset of polarization states distributed uniformly throughout the entire volume of the Poincaré sphere.

We used the dataset to train a fully-connected deep neural network for reconstructing the polarization state given the associated count distribution. The trained network, consisting of 250 neurons per 4 hidden layers, performs a nonlinear transformation on the count distribution and returns four real-valued outputs. These represent elements of a two-by-two triangular matrix τ with real-valued diagonal entries and a single complex off-diagonal entry. Utilizing the Cholesky decomposition, we can reconstruct a Hermitian positive-definitive matrix $\rho = \tau\tau^\dagger$. Upon normalizing its trace to unity, ρ represents a physically sound coherence matrix of the polarization state [29], mathematically equivalent to a density matrix in quantum physics. Therefore, the complete model can be interpreted as providing the polarization coherence matrix of the collected light given the measured count distribution.

We trained the network using the Adam optimizer and a mean squared error loss function. Various hyperparameters, including network architecture, were fine-tuned to optimize the network performance. For this purpose, we employed a validation set, separated from the training data, to find the optimal hyperparameter combination with respect to a fidelity metric $F = \text{Tr}[\sqrt{\sqrt{\rho} \cdot \sigma \cdot \sqrt{\rho}}]^2 \in [0, 1]$, where ρ is the polarization coherence matrix provided by the network and σ is the ground truth matrix of the input polarization state. This metric, which quantifies the closeness between the states, can also be expressed in terms of error as infidelity $1 - F$. The optimized and fully-trained network was evaluated on a test set of previously unobserved polarization states, achieving the unprecedented infidelity of $(9 - 8 + 11) \times 10^{-4}$ as an average with the 10th and 90th percentile. Notably, this outstanding performance shows remarkable stability for over a week without requiring additional calibration or network retraining. Furthermore, for a 1 mm long fiber providing sufficient intermodal interference, we expect an additional improvement in stability of one to two orders of magnitude.

3. PERFORMANCE EVALUATION

We highlight that our approach eliminates the need for capturing an image of the complete speckle pattern. Instead, we collect a limited number of isolated samples, which are then propagated through the fiber array channels. This substantial reduction in data collection allows for sensitive measurements at extremely low intensities using single-photon detectors. To assess the sensitivity of our approach to the processed portion of the speckle pattern, we investigate the achievable infidelity with regard to the number of employed detection channels. Following the same procedure, we trained additional networks utilizing only a subset of the detection channels as inputs. The infidelities achieved by these networks on corresponding test sets are depicted in Fig. 2 (a). The values represent the averaged errors across multiple trained networks, each employing a distinct combination of detection channel subsets. The results illustrated in this graph unequivocally demonstrate that extracting only a few samples from the speckle pattern provides sufficient information about the polarization state.

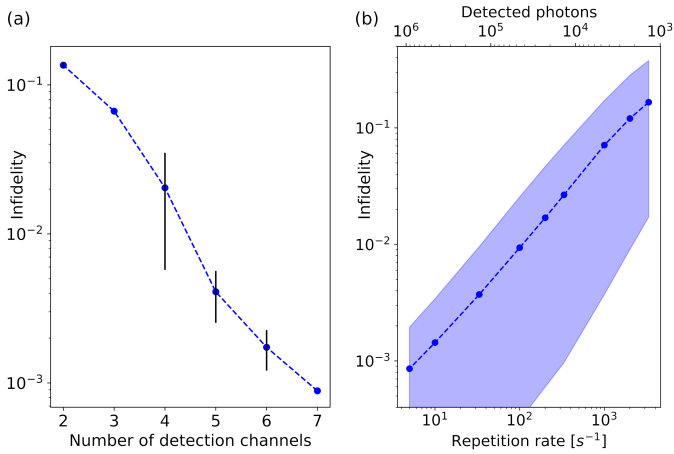


Fig. 2. (a) Polarization error quantified by infidelity for varying numbers of active detectors. Variability bars represent uncertainties arising from different subset combinations. The achieved infidelities underscore the sufficiency of sparse sampling of the speckle pattern. (b) The relation between polarization infidelity, the number of detected photons, and the measurement repetition rate. The colored area indicates the confidence interval of the test set. Given infidelities can be maintained even at significantly higher repetition rates by appropriately adjusting the incident light intensity.

We also explored the impact of the measurement repetition rate on the polarization sensing accuracy. Fig. 2 (b) displays the polarization infidelities of a single network, using all seven channels, evaluated for numerous repetition rates. Notably, achieving an average fidelity of 0.996 at a 33 Hz rate holds particular significance. This frequency aligns closely with the borderline on a perceptible frame rate of the human eye. Hence, it underscores the ability of the sensor to operate in real-time sensing applications with high precision. Furthermore, our setup demonstrates the capacity to measure over 500 polarization states per second while maintaining an average fidelity surpassing 0.95. It is crucial to emphasize that these performances depend on the number of detected photons rather than the repetition rate alone. Consequently, even significantly higher rates can attain the same fidelities with appropriately increased light intensity limited virtually only by saturation of employed single-photon detectors. This feature proves especially beneficial for applications requiring high-repetition-rate sensing. In summary, our polarization sensor represents an outstanding instrument for efficient and accurate real-time polarization microendoscopy and other high-speed polarimetry applications.

To demonstrate the sensing abilities of our approach, we applied our polarization sensor to conduct polarization-sensitive scans of an optically anisotropic specimen. We positioned the sensor tip close to a piece of dense connective tissue (AmScope PS25W). We scanned over its area and characterized the detected polarization using our sensor. The reconstructed polarization states were expressed as three Bloch parameters, i.e., renormalized Stokes parameters [29], and visualized through false-colored RGB images. In Fig. 3, we present this polarization scan in a side-by-side comparison with an intensity image captured from an identical region of the sample. The intensity image was obtained using a monochrome camera (ImagingSource DMK 23U274) with a pixel size of $4.4 \times 4.4 \mu\text{m}$. We illuminated the specimen with a $0.8 \mu\text{m}$ light and projected the resulting im-

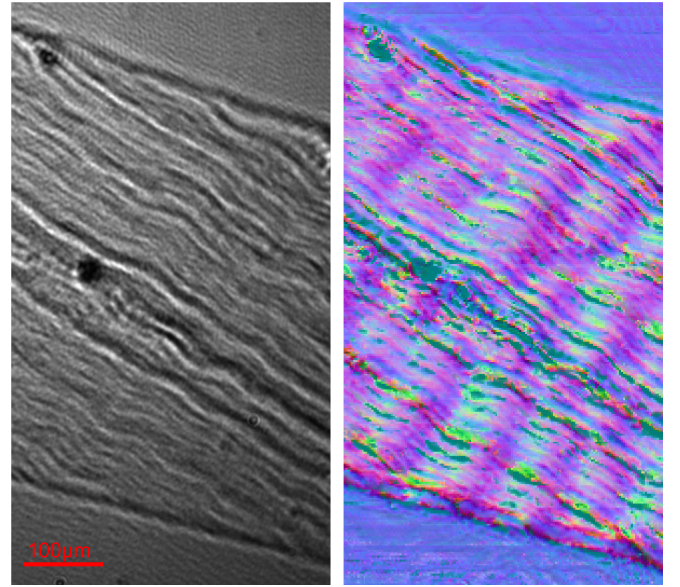


Fig. 3. Visualization of dense connective tissue: (left) intensity image and (right) a scan using the all-fiber polarization sensor. The resulting Bloch parameters are represented as an RGB false-colored image. The latter approach unveils hidden structures not visible in the intensity image.

age onto the camera sensor through a 25.4 mm focal-length lens, providing an estimated fivefold magnification. As Fig. 3 shows, polarized light imaging reveals underlying phase structures hidden from the intensity profile. This showcase not only validates the potential of using our polarization sensor for various sensing applications but also further underscores its invaluable contributions to precise polarization measurements. Our work has cleared the path for highly accurate polarization sensing, even under the most challenging conditions encountered during microendoscopic procedures.

4. CONCLUSION

We have developed a single-shot polarization sensor based on light propagation through a short piece of a few-mode fiber, resulting in a polarization-dependent speckle pattern. The defining aspect of our approach is the sparse sampling of this pattern using a fiber array instead of capturing the whole intensity profile. This characteristic allows the use of any photonic detectors, including single-photon detectors, enabling fast response and operation at low light intensities. The implementation of deep learning algorithms in the system ensures an accurate reconstruction, providing complete information about the polarization state, including partial polarization, with a fidelity surpassing 0.999. This performance shows unprecedented long-term stability exceeding a week. Moreover, shortening the few-mode fiber length to millimeters would extend this stability to several months while maintaining sufficient intermodal coupling. Complemented by the high operation speed, it allows for both real-time endoscopy and high-repetition-rate polarization sensing with remarkable precision. The all-fiber sensor, featuring a compact design with no moving components, is particularly well-suited for reducing the invasiveness of biomedical procedures in constrained spaces. Furthermore, we can enhance the spatial resolution of our sensor by tapering the fiber tip. This method could even provide comparable resolution as near-field

scanning optical microscopy while preserving the single-photon polarization sensitivity. In the view of optically-assisted machine learning, the random propagation in multimode fiber followed by a computational neural network represents an instance of an extreme learning machine or reservoir computing [19, 32]. By demonstrating the single-photon sensing capability of these architectures, we have provided the foundation for decreasing energy consumption in optical sensing and computing. In summary, our polarization sensor significantly advances the field, offering a combination of compactness, accuracy, low light sensitivity, and high operational speed that opens up new possibilities across various applications.

Funding. This work was supported by the Czech Science Foundation (project 21-18545S). MB and DV acknowledge the support by Palacký University (project IGA-PrF-2023-006).

Acknowledgments. We acknowledge the use of cluster computing resources provided by the Department of Optics, Palacký University Olomouc. We thank Jan Provazník for maintaining the cluster and providing support. We also thank Josef Hloušek for developing a 3D model shown in Fig. 1 and Jaromír Běhal for a fruitful discussion on birefringent biological samples.

Disclosures. The authors declare no conflicts of interest.

Data Availability Statement. The code and data that support the findings of this study are publicly available on GitHub [33].

REFERENCES

1. S. Rotter and S. Gigan, "Light fields in complex media: Mesoscopic scattering meets wave control," *Rev. Mod. Phys.* **89**, 015005 (2017).
2. J. Bertolotti and O. Katz, "Imaging in complex media," *Nat. Phys.* **18**, 1008–1017 (2022).
3. H. Cao, A. P. Mosk, and S. Rotter, "Shaping the propagation of light in complex media," *Nat. Phys.* **18**, 994–1007 (2022).
4. K. Vynck, R. Pierrat, R. Carminati, L. S. Froufe-Pérez, F. Scheffold, R. Sapienza, S. Vignolini, and J. J. Sáenz, "Light in correlated disordered media," *Rev. Mod. Phys.* **95**, 045003 (2023).
5. E. Valent and Y. Silberberg, "Scatterer recognition via analysis of speckle patterns," *Optica* **5**, 204–207 (2018).
6. M. W. Matthès, Y. Bromberg, J. de Rosny, and S. M. Popoff, "Learning and avoiding disorder in multimode fibers," *Phys. Rev. X* **11**, 021060 (2021).
7. T. Čižmár and K. Dholakia, "Exploiting multimode waveguides for pure fibre-based imaging," *Nat. Commun.* **3**, 1027 (2012).
8. M. Plöschner, T. Tyc, and T. Čižmár, "Seeing through chaos in multimode fibres," *Nat. Photonics* **9**, 529–535 (2015).
9. N. Borhani, E. Kakkava, C. Moser, and D. Psaltis, "Learning to see through multimode fibers," *Optica* **5**, 960–966 (2018).
10. Y. Li, Y. Xue, and L. Tian, "Deep speckle correlation: a deep learning approach toward scalable imaging through scattering media," *Optica* **5**, 1181–1190 (2018).
11. B. Rahmani, D. Loterie, G. Konstantinou, D. Psaltis, and C. Moser, "Multimode optical fiber transmission with a deep learning network," *Light. Sci. & Appl.* **7**, 69 (2018).
12. P. Caramazza, O. Moran, R. Murray-Smith, and D. Faccio, "Transmission of natural scene images through a multimode fibre," *Nat. Commun.* **10**, 2029 (2019).
13. B. Rahmani, D. Loterie, E. Kakkava, N. Borhani, U. Teĭin, D. Psaltis, and C. Moser, "Actor neural networks for the robust control of partially measured nonlinear systems showcased for image propagation through diffuse media," *Nat. Mach. Intell.* **2**, 403–410 (2020).
14. R. Ziv, A. Dikopoltsev, T. Zahavy, I. Rubinstein, P. Sidorenko, O. Cohen, and M. Segev, "Deep learning reconstruction of ultrashort pulses from 2d spatial intensity patterns recorded by an all-in-line system in a single-shot," *Opt. Express* **28**, 7528–7538 (2020).
15. W. Xiong, B. Redding, S. Gertler, Y. Bromberg, H. D. Tagare, and H. Cao, "Deep learning of ultrafast pulses with a multimode fiber," *APL Photonics* **5**, 096106 (2020).
16. H. Defienne, M. Barbieri, I. A. Walmsley, B. J. Smith, and S. Gigan, "Two-photon quantum walk in a multimode fiber," *Sci. Adv.* **2**, e1501054 (2016).
17. S. Leedumrongwatthanakun, L. Innocenti, H. Defienne, T. Juffmann, A. Ferraro, M. Paternostro, and S. Gigan, "Programmable linear quantum networks with a multimode fibre," *Nat. Photonics* **14**, 139–142 (2020).
18. N. H. Valencia, S. Goel, W. McCutcheon, H. Defienne, and M. Malik, "Unscrambling entanglement through a complex medium," *Nat. Phys.* **16**, 1112–1116 (2020).
19. D. Pierangeli, G. Marcucci, and C. Conti, "Photonic extreme learning machine by free-space optical propagation," *Photonics Res.* **9**, 1446–1454 (2021).
20. B. Courme, P. Cameron, D. Faccio, S. Gigan, and H. Defienne, "Manipulation and certification of high-dimensional entanglement through a scattering medium," *PRX Quantum* **4**, 010308 (2023).
21. B. Redding, S. F. Liew, R. Sarma, and H. Cao, "Compact spectrometer based on a disordered photonic chip," *Nat. Photonics* **7**, 746–751 (2013).
22. R. K. Gupta, G. D. Bruce, S. J. Powis, and K. Dholakia, "Deep learning enabled laser speckle wavemeter with a high dynamic range," *Laser & Photonics Rev.* **14**, 2000120 (2020).
23. M. Juhl and K. Leosson, "Polarimetry with disordered photonic structures," *ACS Photonics* **7**, 203–211 (2020).
24. M. Facchin, G. D. Bruce, and K. Dholakia, "Speckle-based determination of the polarisation state of single and multiple laser beams," *OSA Continuum* **3**, 1302–1313 (2020).
25. N. A. Rubin, P. Chevalier, M. Juhl, M. Tamagnone, R. Chipman, and F. Capasso, "Imaging polarimetry through metasurface polarization gratings," *Opt. Express* **30**, 9389–9412 (2022).
26. D. Pierangeli and C. Conti, "Single-shot polarimetry of vector beams by supervised learning," *Nat. Commun.* **14**, 1831 (2023).
27. M. Stibůrek, P. Ondráčková, T. Tučková, S. Turtaev, M. Šiler, T. Pikálek, P. Jákl, A. Gomes, J. Krejčí, P. Kolbábková, H. Uhlířová, and T. Čižmár, "110 μm thin endo-microscope for deep-brain in vivo observations of neuronal connectivity, activity and blood flow dynamics," *Nat. Commun.* **14**, 1897 (2023).
28. S. Goel, C. Conti, S. Leedumrongwatthanakun, and M. Malik, "Referenceless characterization of complex media using physics-informed neural networks," *Opt. Express* **31**, 32824–32839 (2023).
29. S. Huard, *Polarization of Light* (Wiley, 1997).
30. M. Bielak, R. Stárek, V. Krčmarský, M. Mičuda, and M. Ježek, "Accurate polarization preparation and measurement using twisted nematic liquid crystals," *Opt. Express* **29**, 33037–33052 (2021).
31. D. Vařinka, M. Bielak, M. Neset, and M. Ježek, "Bidirectional deep learning of polarization transfer in liquid crystals with application to quantum state preparation," *Phys. Rev. Appl.* **17**, 054042 (2022).
32. P. Mujal, R. Martínez-Peña, J. Nokkala, J. García-Beni, G. L. Giorgi, M. C. Soriano, and R. Zambrini, "Opportunities in quantum reservoir computing and extreme learning machines," *Adv. Quantum Technol.* **4**, 2100027 (2021).
33. D. Vařinka, "Github repository," <https://github.com/VasinkaD/Polarization-Deep-Sense> (2024).